Available online at www.sciencedirect.com
SCIENCE DIRECT®
Cement & Concrete Composites 27 (2005) 758–768
Cement & Concrete Composites
www.elsevier.com/locate/cemconcomp

Air-foamed calcium aluminate phosphate cement for geothermal wells

T. Sugama [a,*], L.E. Brothers [b,1], T.R. Van de Putte [c]

[a] Brookhaven National Laboratory, Building 526, 12 N. Sixth St. Upton, NY 11973, USA
[b] Halliburton 2600 S. 2nd Steet, P.O. Drawer 1431 Duncan, OK 73536, USA
[c] CalEnergy Operating Corporation, 7030 Gentry Rd. Calipatria, CA 92233, USA

Received 30 August 2004; accepted 10 November 2004

Abstract

Air-foamed low-density calcium aluminate phosphate (CaP) cement slurry was prepared by mixing it with chemical foaming reagent at room temperature without any pressure, followed by autoclaving at 200 °C. When the porosity, compressive strength, and water permeability of the autoclaved CaP foam cement made from a 1.22 g/cc slurry density was compared with those of N_2 gas-foamed Class G cement made from a slurry of similar density under high pressure and hydrothermal temperature at 288 °C, the CaP cement revealed some advanced properties, such as a higher compressive strength and lower porosity. These advanced properties were due to the hybrid formation of three crystalline hydrothermal reaction products; hydroxyapatite, boehmite, and hydrogarnet phases. However, one shortcoming was an increase in water permeability because of the formation of an undesirable continuous porous structure caused by coalesced air bubble cells, suggesting that an appropriate lesser amount of foaming reagent be used to create a conformation in which fine discrete air-bubble cells are uniformly dispersed throughout the slurry. For non-foamed cement, three major factors contributed to protecting carbon steel against corrosion: (1) good adherence to steel, reflecting a high extent of coverage by the cement layer over the steel's surfaces; (2) retardation of cathodic corrosion reactions; and, (3) minimum conductivity of corrosive ionic electrolytes. However, adding an excessive amount of foaming reagent did not offer as effective corrosion protection as that of non-foamed cement.

Keywords: Calcium aluminate phosphate cement; Air-foamed cement slurry; Geothermal well; Corrosion protection

1. Introduction

In pumping and circulating a cement slurry of typical density, 1.9–2.0 g/cc, used in geothermal wells, there is a considerable risk of creating undesirable fracture zones in a weak unconsolidated rock foundation with very fragile gradients due to the high hydrostatic pressure that is required to circulate such dense slurry, thereby causing the problem of lost circulation. Thus, it is very important to use cement slurry with the minimum density responsible for reducing this hydrostatic pressure, so minimizing the possibility of experiencing lost circulation.

There are three ways to prepare the low-density slurries with calcium aluminate phosphate (CaP) geothermal well cement: First is to incorporate pressure- and high temperature-resistant hollow ceramic-shelled microspheres, with a density of ~0.7 g/cc and a particle size of 75–200 μm, into the slurry; the second is to disperse fine N_2 gas bubbles created by injecting highly

* Corresponding author. Fax: +1 631 344 2359.
E-mail addresses: sugama@bnl.gov (T. Sugama), Lance.Brothers@halliburton.com (L.E. Brothers), Todd.VandePutte@calenergy.com (T.R. Van de Putte).
[1] Fax: +1 405 251 4745.

0958-9465/$ - see front matter © 2005 Elsevier Ltd. All rights reserved.
doi:10.1016/j.cemconcomp.2004.11.003

pressured N_2 into a slurry containing the foaming additive; and, the third is to introduce small, fine air bubbles into the slurry by adding a foaming reagent to it. For the first method, we reported that among the various ceramic microspheres available, an aluminosilicate-shelled hollow microsphere was most suitable for the CaP cement; it provided a low-density slurry of ~1.3 g/cc in conjunction with a compressive strength of more than 6.89 MPa [1]. Regarding the second method, the N_2 gas-foamed CaP cement slurry was successfully placed in Coso geothermal wells at temperature range of 160–200 °C in the USA by a reverse circulation placement technique (RCPT) in 2002. Almost two years after it was placed, Moore, et al. reported that this foamed cement retained its integrity by showing a great adherence to the casing pipes, and displaying both good mechanical and physical behavior [2]. In addition, the N_2-foamed cement served as an excellent thermal insulator and corrosion inhibitor for geothermal steam production pipes [3].

Although the N_2-foamed CaP cement slurry has offered very promising results thus far, the third method using a simple foaming reagent was thought of as the most cost-effective and inexpensive technology because it eliminated the use of expensive ceramic microspheres and the time-consuming, complicated N_2-injection process. The microscale air bubble cells are simply created within the slurry by adding a certain amount of foaming reagent to it, and can be dispersed uniformly in it by mixing in a shear blender at room temperature. Using the same foaming technology, an aerosol foam cement in terms of the cellular cement containing air bubbles of more than 50% of the volume was widely applied to the building materials encompassing lightweight cores in a sandwich structure, thermal insulators, sound barriers, fire wall, structural backfill, and foundations because of its good creep resistance, high specific stiffness and strength [4–6], low thermal conductivity [7], and good freeze–thaw durability [8]. However, there are four important issues to be addressed before this technology is applied to geothermal wells: The first concerns the stability of air bubble cells dispersed in the slurry under a high hydrothermal temperature; second are the changes in the mechanical and physical properties of set foam cement as a function of the extent of foaming; third is whether the crystalline phase composition responsible for strengthening the cement is changed by varying the content of foaming reagent; and, fourth is the effectiveness of foamed cement in mitigating corrosion of carbon steel casing pipes.

In response to these questions, we established six research objectives (1) to determine the changes in porosity, water permeability, and compressive strength of autoclaved foam cement as a function of content of foaming reagent, (2) to identify the crystalline phases formed in the non-foamed and foamed cements after autoclaving, (3) to explore the microstructure developed within foamed cement, (4) to use the DC electrochemical potentiodynamic polarization test on carbon steel coupons covered with foamed cements, (5) to measure the ionic conductivity of foamed cement layers deposited on the steel's surfaces by AC electrochemical impedance spectroscopy (EIS), and (6) to determine the adherence of foamed cement to the surface of steel.

2. Experimental procedure

2.1. Materials

Halliburton supplied the cocoamidopropy dimethylamine oxide-based foaming reagent under the trade name "ZoneSealant 2000". Calcium aluminate cement (CAC, Secar 60) and type F fly ash, used as the solid reactants, were obtained from the Lafarge Aluminate Corp., and Pozament Corp., respectively. A 25 wt.% sodium polyphosphate $-[-(NaPO_{3-})_{n-}$, NaP], supplied by the Aldrich Chemical Company Inc., was used as the cement-forming liquid reactant for modifying the CAC-blended fly ash solid reactant. The solid reactant, made up in a twin shell dry blender, had a constant ratio of CAC/fly ash of 60/40 by weight. The weight ratio of the 25 wt.% NaP solution to the blend cement for the original cement slurry was 0.5. In preparing the foamed slurries, 0, 0.5, 1.0, 1.5, 2.0, 3.0, 4.0, 5.0, 6.0, 7.0, 10.0, 15.0, and 20.0% foaming reagent by weight of total water in the 25 wt.% NaP solution was added to the original slurry, and then was mixed by shear-blender. This shear mixing led to the aeration of slurry by increasing the incorporation of air bubbles into the slurry, and we observed that the originally stiff slurry was converted into a smooth creamy one.

2.2. Measurements

The density, g/cc, of the foamed cement slurries was determined 10 min after mixing using the fluid density balance. Then, the slurries were poured into two different cylindrical sized molds: One was 30-mm diameter× 60-mm long for measuring compressive strength and porosity; the other was 30-mm diam. 33-mm long for testing water permeability. The slurry-filled molds were left for 24 h at room temperature, and then the hardened cement specimens were removed from the molds and autoclaved for 24 h at 200 °C, which is the maximum temperature at location that the formed CaP cements were placed in geothermal wells thus far. The porosity of autoclaved cements was measured by helium comparison pyconometry. Water permeability through the cylindrical cement specimens under the pressure of 202.65 kNm^{-2} was determined by the Ruska liquid permeameter. The results of these tests and measurements are the average

from three specimens. Changes in the crystalline phase composition of autoclaved cements with different contents of foaming reagent were studied by X-ray diffraction (XRD). Scanning electron microscopy (SEM) was used to explore the microstructure developed in the foamed cements, and to reveal the morphological features of the underlying steel's surfaces after physically removing the autoclaved cement layers. For the latter, the chemistry of their surface was surveyed by the energy-dispersive X-ray spectrum (EDX) to obtain information on the extent of adherence of the foamed cement to steel's surface. DC electrochemical testing for corrosion was performed with the EG & G Princeton Applied Research Model 362-1 Corrosion Measurement System. The electrolyte was a 1.0 M sodium chloride. The specimen was mounted in a holder, and then inserted into an EG & G Model K47 electrochemical cell. The test was conducted under an aerated condition at 25 °C, on an exposed surface area of 1.0 cm^2. The polarization curves were measured at a scan rate of 0.5 mVs^{-1} in the corrosion potential range from −1.35 to −0.75 V. AC electrochemical impedance spectroscopy (EIS) was used to evaluate the ability of the exposed cement layers to protect the steel from corrosion. The specimens were mounted in a holder, and then inserted into an electrochemical cell. Computer programs were prepared to calculate theoretical impedance spectra and to analyze the experimental data. The specimens with a surface area of 13 cm^2 were exposed to an aerated 1.0 M sodium chloride electrolyte at 25 °C, and single-sine technology with an input AC voltage of 10 mV (rms) was employed over a frequency range of 10 KHz to 10^{-2} Hz. To estimate the protective performance of the coatings, the pore resistance, R_p, (Ωcm^2) was determined from the plateau in Bode-plot scans that occurred in low frequency regions.

3. Results and discussion

3.1. Mechanical and physical properties

Table 1 lists the changes in slurry's density, and in the porosity, compressive strength, and water permeability of autoclaved non-foamed and foamed cements as a function of the content of foaming reagent. The data showed that the slurry's density sharply dropped between 0 and 5 wt.% contents of the foaming reagent; beyond that, it gradually declined with an increase in the reagent's content. In fact, the density of non-foamed slurry fell as much as 30% to 1.34 g/cc when a 5 wt.% foaming reagent was added. Adding 20 wt.% reagent led to a considerable reduction in density to 1.01 g/cc; however, this value was only ~25% lower than that of the 5 wt.% reagent. Nevertheless, this foaming reagent significantly reduced the density of the CaP cement's slurry. After the foamed slurries were autoclaved for 24 h at 200 °C, all the air bubble cells were converted into copious pores that were distributed throughout the set cements. Thus, the porosity of autoclaved cements depended primarily on the slurry's density; their porosity increased with reducing density. The porosity of 10.9% for the non-foamed cement rose more than five times when 20 wt.% reagent was added. Correspondingly, the water permeability of the autoclaved cements was strikingly enhanced with an increasing content of foaming reagent. The non-foamed cement made from the slurry density of 1.91 g/cc had a very low water permeability of 2.0×10^{-5} Darcy. When the slurry was foamed by adding 1.0 wt.% reagent to give a 1.65 g/cc density, it still retained water permeability at a low level of 4.9×10^{-5} Darcy. However, adding a 3.0 wt.% reagent accompanying the 1.43 g/cc density engendered a notable increase in the extent of water transport; in fact, its permeability was nearly two orders of magnitude as high as that of the 1.0 wt.% reagent. A further reduction of the slurry's density allowed the water to permeate more easily through the cement; thus, adding more than 5 wt.% of reagent led to a very high permeability of 10^{-2} Darcy. As expected, the compressive strength of 200 °C-autoclaved lightweight cements weakened with decreasing density of slurries because of the increase in porosity. The compressive strength of non-foamed cement fell ~40% to 43.4 MPa with 1 wt.% reagent. A further reduction to 24.1 MPa was observed from the 3 wt.% reagent-foamed cement. With the addition of more than 5 wt.%, the developed strength was less than 20 MPa.

Table 1
Changes in the density of the slurries, and in the porosity, compressive strength, and water permeability of 200 °C-autoclaved CaP foam cements as a function of the content of the foaming reagent

Foaming reagent, wt.%	Density of slurry, g/cm^3	Porosity of autoclaved cement, %	Compressive strength of autoclaved cement, MPa	Water permeability of autoclaved cement, Darcy
0	1.91	10.94	72.8	2.0×10^{-5}
1	1.65	27.80	43.4	4.9×10^{-5}
3	1.43	38.50	24.1	1.6×10^{-3}
5	1.34	43.80	18.5	2.0×10^{-2}
10	1.22	49.30	14.7	4.9×10^{-2}
15	1.11	54.35	11.0	7.6×10^{-2}
20	1.01	60.49	6.8	8.7×10^{-2}

Hence, the cement made with the lowest density of 1.01 g/cc had a very low compressive strength of 6.8 MPa.

Using N_2-foaming technology, Harms and Febus stated that the 1.2 g/cc density-derived Class G foam cement used in the steam injection wells had a porosity of 75% and compressive strength of 8.3 MPa after 20 days exposure at 288 °C [9]. Montman et al. reported that a 1.2 g/cc density-derived Class H foam cement possessing a water permeability of 2.3×10^{-3} Darcy was successfully used in oil wells [10]. With a lower density Class H cement slurry of 0.96 g/cc, the set cement had a compressive strength of 4.5 MPa and a water permeability of 3.1×10^{-2} Darcy after exposure for 3 days at 60 °C [11]. Relating this information to our data, the shortcoming of air-foamed cement was its higher water permeability compared with that of N_2-foamed cement, although the hydrothermal temperature, exposure time, and cement species were different. For instance, the water permeability of the air-foamed CaP cement made from ~1.2 g/cc slurry density after 1 day exposure at 200 °C was 4.9×10^{-2} Darcy, corresponding to almost the one order of magnitude higher than that of N_2-foamed Class G cement made with the same slurry density after 20 days at 288 °C. However, the compressive strength and porosity of air-foamed CaP cement was somewhat higher and lower, respectively, than those of N_2-foamed Class G cement.

3.2. Development of microstructure

Our attention next focused on exploring the microstructure developed in the foamed cement. The ideal microstructure of foamed lightweight cement in minimizing the extent of water transportation would be to have a uniform distribution of discrete micro-size pores generated from the fine air-bubbles in the slurry. In contrast, it appears that the coalescence of many large-size pores may create an undesirable microstructure, causing a high degree of water transportation. To validate this concept, we explored by SEM the fractured surfaces of the two foamed cements made with the slurry densities of 1.43 and 1.11 g/cc, respectively (Fig. 1). With a 1.43 g/cc, the image (left) revealed a microstructure consisting of uniform distribution of discrete pores, ranging from as large as ~290 μm to as small as ~40 μm. In contrast, a quite different microstructure was observed in the cement made with the 1.11 g/cc (right). The image revealed that the undesirable coalescence resulted in a connected pore structure, allowing water to permeate easily through the cement. One possibility for the development of such an undesirable pore structure was the incorporation of excessive numbers of air bubble cells after adding an excess of reagent to the slurry, leading to the coalescence of the bubbles. Relating this information to the cement's mechanical and physical properties, it is possible to assume that the bubble cells created by the N_2 gas-foaming technology under a high pressure probably are smaller than the air-foamed bubble cells generated without pressure, thereby minimizing the extent of their coalescence.

3.3. Phase identification

One concern in using the chemical foaming reagent was whether it would change the composition of the crystalline phases as hydrothermal reaction products responsible for strengthening the set CaP cement. To obtain this information, XRD was used to identify the phases assembled in the non-foamed cement, and in the 5 and 20 wt.% reagent-foamed cements after autoclaving at 200 °C. Fig. 2 depicts the XRD traces for these powder samples. For non-foamed cement, the XRD pattern (a) showed that the cement was composed of three crystalline hydration reaction products: hydroxyapataite, [$Ca_5(PO_4)_3(OH)$, HOAp]; boehmite,

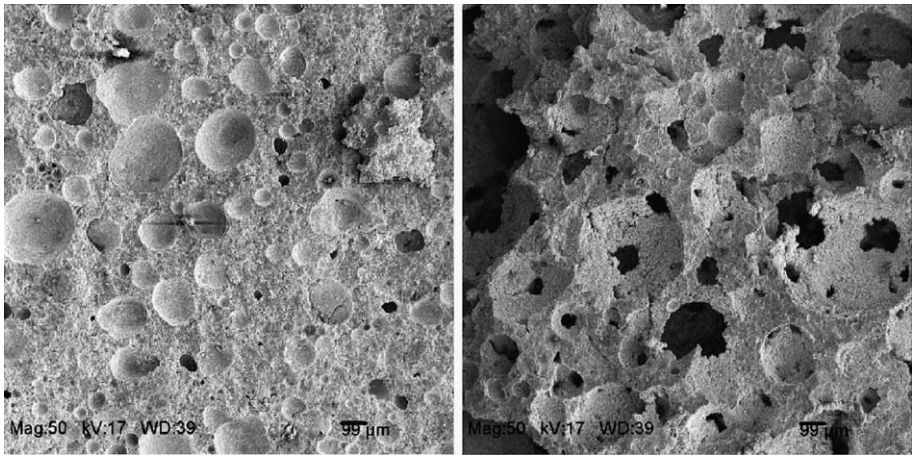

Fig. 1. SEM images of the fractured surfaces of foam cements made from slurry densities of 1.42 (left) and 1.11 g/cc (right).

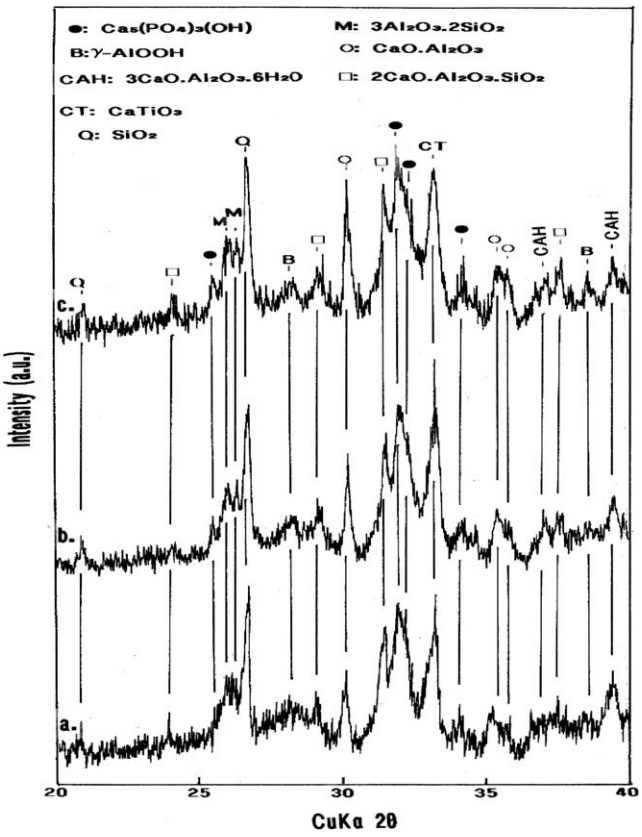

Fig. 2. XRD patterns for (a) non-foamed cement, and (b) 5 wt.%, and (c) 20 wt.% reagent-foamed cements after autoclaving at 200 °C.

(γ-AlOOH); and hydrogarnet, ($3CaO \cdot Al_2O_3 \cdot 6\,H_2O$, C_3AH_6). These reaction products appear to act as cementitious phases, and bind together all the non-reacted and partially reacted cement particles into cohesive mass, thereby developing the strength of autoclaved cement. There also were five remaining non-reacted phases originating from the two solid counter reactants to the liquid NaP reactant: quartz (SiO_2) and mullite ($3Al_2O_3 \cdot 2SiO_2$) arose from the Class F fly ash; and monocalcium aluminate ($CaO \cdot Al_2O_3$, CA), gehlenite ($2CaO \cdot Al_2O_3 \cdot SiO_2$, C_2AS) and pervoskite ($CaTiO_3$) from the Secar 60 CAC. The features of the XRD pattern (b) from the 5 wt.% reagent-foamed cement closely resembled that of the non-foamed cement, except for the growth in line intensity of the non-reacted monocalcium aluminate (CA) phase. Since the major phase in the Secar 60 CAC reactant is CA, it is possible to rationalize that adding foaming reagent to the cement slurry restrains the reactions between the CA and the NaP solution that form HOAp, γ-AlOOH, and C_3AH_6. In fact, as more foaming reagent was incorporated up to 20 wt.%, the line intensity of CA became much stronger than that seen in 5 wt.% foaming reagent, while the same reaction products as those from the non-foamed and 5 wt.% foamed cements were formed as demonstrated in the XRD pattern (c). Nevertheless, the foaming reagent appears to inhibit the reactions between CA and NaP. However, it is very difficult to determine the extent of its inhibition as well as to understand its inhibiting mechanisms from this limited information.

3.4. Corrosion protection

Based upon our results showing that the degree of water permeability and the development of undesirable continuous pore structure depended mainly on the content of foaming reagent, a considerable attention centered on assessing the ability of foamed cements to protect the underlying carbon steel against brine-induced corrosion. This information was obtained by three methods: (1) Tafel extrapolation technique on DC potentiodynamic polarization diagrams; (2) image and chemical analyses of the interfacial steels' surfaces by SEM–EDX; and, (3) AC electrochemical impedance spectroscopy (EIS) to determine the extent of ionic conductivity.

For the first assessment, the cement-coated carbon steel test panels were prepared in the following sequence: First, 65 mm × 65 mm panels were cleaned by an alkaline solution at 70 °C; second, the alkali-cleaned panels were dipped in the non-foamed and foamed cement slurries and then withdrawn; third, the slurry-covered panels were exposed for 24 h in a steam at 200 °C; and finally, the autoclaved cement coatings were left for 24 h in atmospheric environment before the DC potentiodynamic polarization test. The thickness of all the coatings ranged from ~0.4 to ~0.55 mm. Fig. 3 gives the typical cathodic-anodic polarization curves plotting the polarization voltage, E, versus current density, A/cm^2, for the steel panels covered with the non-foamed cement and the foamed cements made with 3 and 20 wt.% reagent. The shape of the curves shows the transition from cathodic polarization at the onset of the most negative potential to the anodic polarization curves at the end of positive potential. The potential axis at the transition point from cathodic to anodic curves is normalized as the corrosion potential, E_{corr}. When compared with the non-foamed cement-coated steel denoted as 0 wt.%, there are two noticeable differences in the curves' features for the steel panels coated with foamed cements: One was a shift in the E_{corr} value to a more negative site with a greater content of foaming reagent, and the other was an enhancement of cathodic current density (A/cm^2) with an increase in its content in the potential region between −0.75 and −0.95 V. Difference (1) directly reflects the extent of coverage of the cement coating over the entire steel surface; namely, the good coverage by a continuous void-free coating layer is responsible for moving the E_{corr} value to a more positive site. Hence, the resulting shift to negative site of E_{corr} demonstrated that the extent of coverage by the foamed cements became poor as the content of foaming reagent

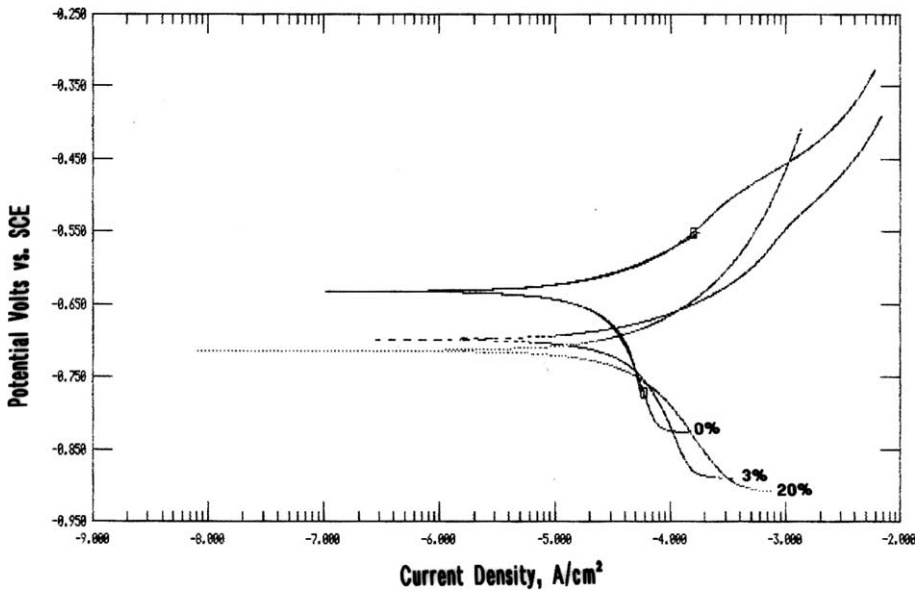

Fig. 3. Potentiodynamic cathodic-anodic polarization diagrams for a non-foamed cement, and 3 wt.% and 20 wt.% reagent-foamed cements.

was increased. This might suggested that the cement layer formed over the steel's surfaces was faulty and non-continuous because of its porous structure. For difference (2), the indication of high value of cathodic current density signifies that the cathodic reaction at the corrosion site of steel is accelerated, particularly the oxygen reduction reaction, $2H_2O + O_2 + 4e^- \rightarrow 4OH^-$. Hence, such a reaction, which leads to the corrosion of steel, appears to be promoted by depositing the foamed cements on the steel's surfaces. Correspondingly, an increase in the content of foaming reagent further accelerated the rate of this reaction, meaning that adding a respectable amount of foaming reagent did not achieve the ultimate corrosion-protective performance of cement.

On the basis of the interpretation of this potentiodynamic polarization curve (Fig. 4), we determined the absolute corrosion rates of steel, expressed in the conventional engineering units of milli-inches per year (mpy). The Eq. (1) proposed by Sterm and Geary[12], was used in the first step:

$$I_{corr} = \beta_a \cdot \beta_c / 2.303(\beta_a + \beta_c) R_p \quad (1)$$

where I_{corr} is the corrosion current density in A/cm^2, β_a and β_c having the units of V/decade of current refer to the anodic and cathodic Tafel slopes, respectively, which were obtained from the log I vs. E plots encompassing both anodic and cathodic regions, and R_p is the polarization resistance which was determined from the corrosion potential, E_{corr}. When I_{corr} was computed through Eq. (1), the corrosion rate (mpy) can be obtained from the following expression:

$$\text{Corrosion rate} = 0.13\, I_{corr}(\text{EW})/d \quad (2)$$

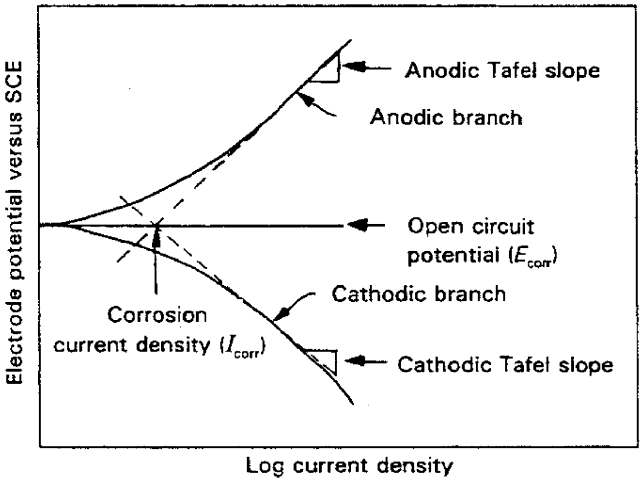

Fig. 4. Typical Tafel plot from a polarization experiment.

where EW is the equivalent weight of the corroding species in g, and d is the density of the corroding species in g/cm^3.

Table 2 gives the I_{corr} and corrosion rate from this Tafel calculation for steel panels coated with the non-foamed cement, and the cements foamed by incorporating 3, 5, 10, and 20 wt.% reagents. The corrosion rate of the steel for non-foamed cement (0 wt.% foaming reagent) was 23.90 mpy accompanying I_{corr} of 5.23×10^{-5} A/cm^2. These values tended to rise when the content of foaming reagent was increased; in fact, the 36.74 mpy and 8.04×10^{-5} A/cm^2 for the cement with 20 wt.% reagent corresponded to an increment of ~54%, compared with those of the non-foamed cement. This finding strongly demonstrated that adding an excessive foaming reagent, which leads to the formation

Table 2
Tafel analyses of potentiodynamic polarization curves for steel panels covered with foamed and non-foamed cements

Foaming reagent, wt.%	E_{corr} ($I = 0$), (V)	β_a, (V/decade)	β_c, (V/decade)	I_{corr}, (A/cm^2)	Corrosion rate, (mpy)[a]
0	−0.6326	0.1291	2.707	5.23×10^{-5}	23.90
3	−0.6987	0.0879	0.4569	5.53×10^{-5}	25.28
5	−0.7074	0.0960	0.4094	6.06×10^{-5}	27.72
10	−0.6898	0.1016	0.5144	7.01×10^{-5}	32.04
20	−0.714	0.1705	0.3565	8.04×10^{-5}	37.74

[a] mpy: milli-inches per year.

of cement with a higher porosity, diminished the maximum effectiveness of the autoclaved cement in protecting the underlying steel against corrosion.

Fig. 5 compares the morphological features of the interfacial steel surfaces after physically removing the non-foamed cement, and the 3, 5, and 20 wt.% reagent-foamed cements at the cement/steel joints, then blasting the surfaces with air compressed at 0.7 MPa. The SEM images revealed that the extent of the surfaces' asperities depends on the content of reagent; its extent seems to decline with an increasing content of reagent. The steel dislodged from the 20 wt.% reagent-foamed cement was characterized by divulging a very smooth texture, compared with the roughness of the interfacial steel surfaces from which the non-foamed and 3 wt.% reagent-foamed cements were removed.

To obtain more detailed images and information on the chemistry of the microstructures developed at interfaces between the cement and steel after autoclaving, each of these interfacial steel surfaces was closely examined by SEM-EDX. Fig. 6 shows the magnified SEM image of the steel site delaminated from the non-foamed

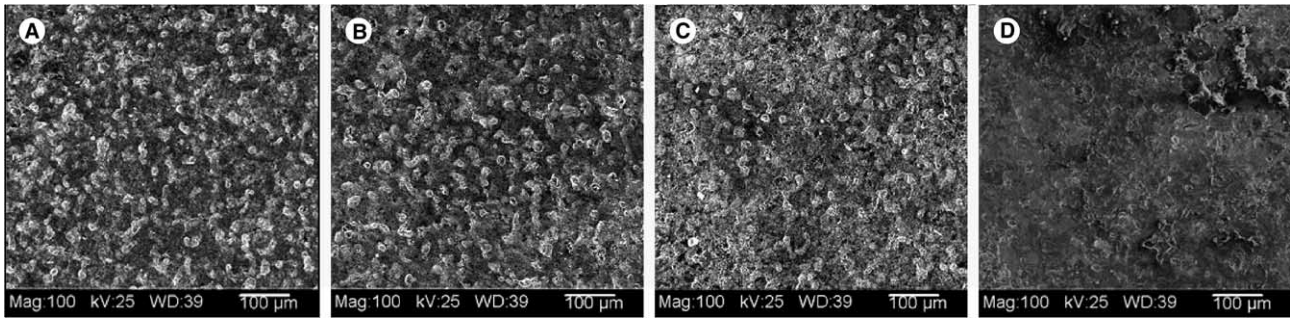

Fig. 5. SEM images of interfacial steel sites after physically removing the following cements: (A) non-foamed cement, and (B) 3 wt.%-, (C) 5 wt.%-, and (D) 20 wt.%-reagent foamed cements.

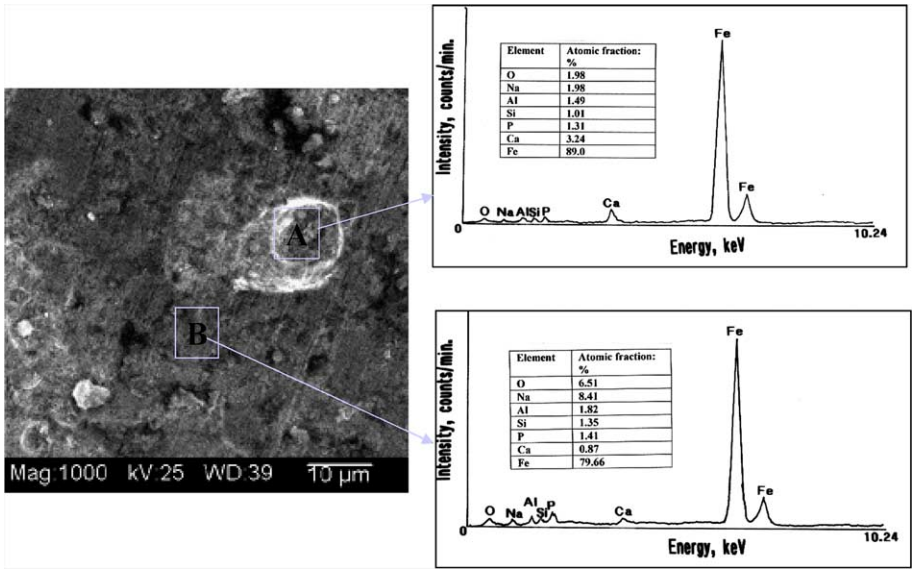

Fig. 6. Highly magnified SEM and EDX spectra of interfacial steel site removed from underneath the non-foamed cement.

cement. The image highlights two distinctive areas: One is a prominent portion denoted as area "*A*", and the other is a relatively smooth area at location "*B*". The EDX spectra for both areas "*A*" and "*B*" included the dominant peak of Fe as the principal element, and weak peaks of Ca, P, Si, Al, Na, and O as the minor elements. Since the penetration depth of the X-rays emitted from EDX is around 2 μm, the atomic fraction computed from the peak counts for each of respective elements is the average percentages of all elements exciting in ~2 μm subsurface layer. We can assume that the Fe atom originates from two resources; the Fe in the oxide compounds occupying the outermost surface sites of steel, and the elemental Fe in the steel. All the other atoms appear to belong to the CaP cement, underscoring the fact that although the layer had been removed, some cement still remained on the steel's surface. Thus, we believe that the non-foamed cement adhered well to the steel, thereby representing that the interfacial bond failure at steel/cement joint took place in the cement layer. A similar image was obtained from the interfacial steel side removed from the 3 wt.% reagent-foamed cement (Fig. 7). Although a substantial penetration depth of the X-ray depended on the difference in porous structures, the EDX spectrum taken from the site "C" showed that the total amount of cement-related atoms was only 5.81%, corresponding to more than two times less than that on the steel's surface from non-foamed cement. So few cement remnants on the steel's surface can be interpreted as demonstrating that the cement foamed by 3 wt.% reagent does not adhere as effective as does the non-foamed cement. A further impairment of its adherent property was observed from the 5 wt.% reagent-foamed cement/steel joints. In fact, the EDX analysis for the interfacial steel site revealed no cement-related elements in some areas (Fig. 8). As

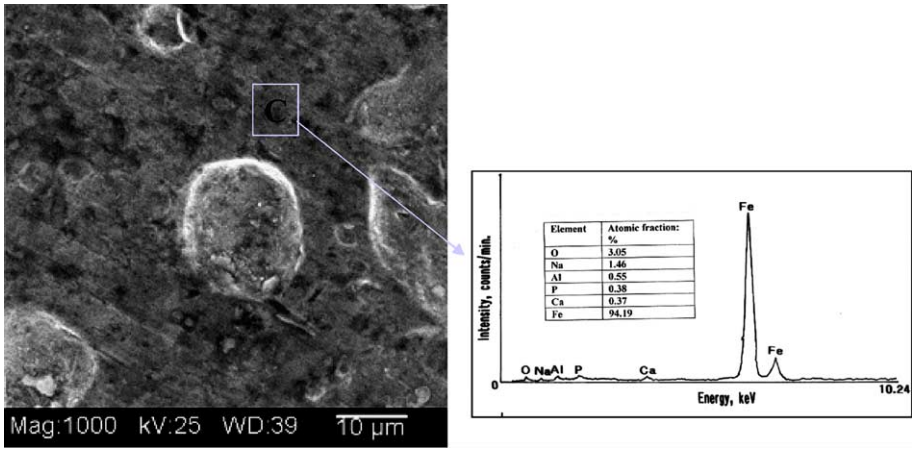

Fig. 7. SEM close-examination and EDX spectrum of interfacial steel site removed from beneath 3 wt.% reagent-foamed cement.

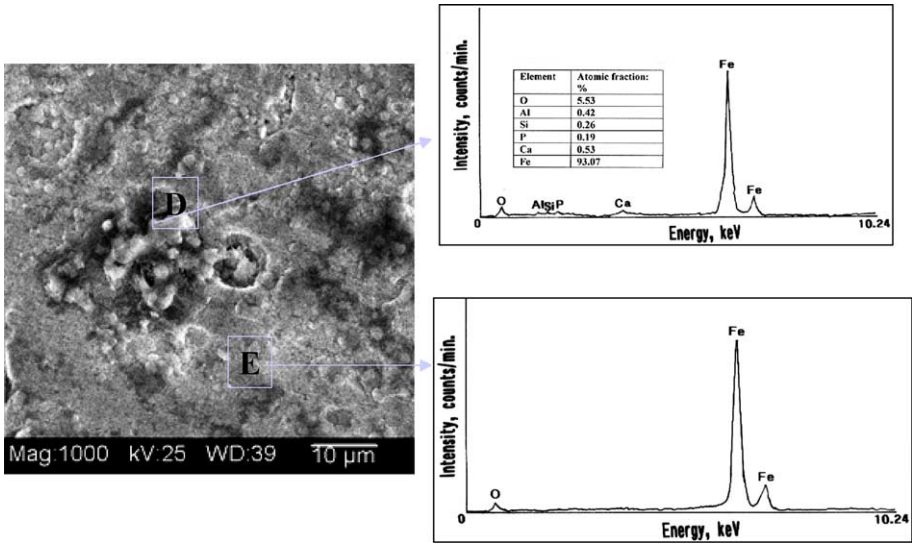

Fig. 8. SEM-EDX analysis of interfacial steel site removed from beneath the 5 wt.% reagent-foamed cement.

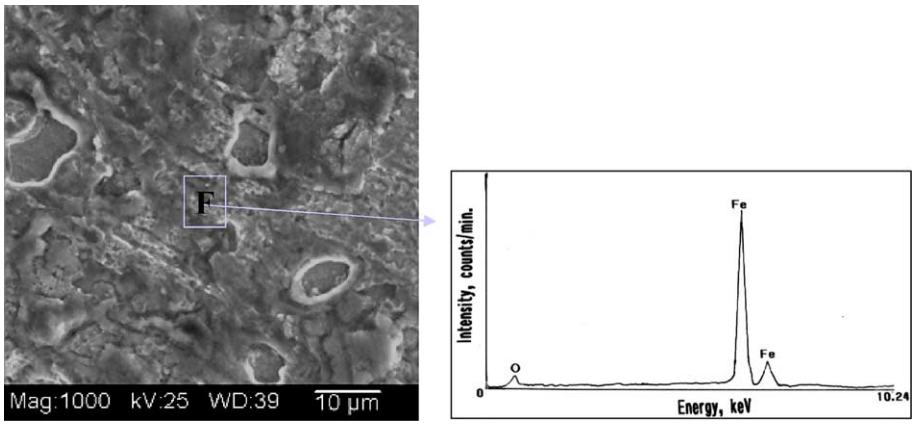

Fig. 9. SEM-EDX analysis of interfacial steel site at 20 wt.% reagent-foamed cement/steel joint.

evident from the image of a very smooth texture, the adherence of the 20 wt.% reagent-foamed cement was extremely poor (Fig. 9); no cement-related elements were detected over the entire surfaces. Relating these findings to the results from the potentiodynamic polarization study, the fact that the adherence of cement decreased with an increasing content of foaming reagent was one of the major reasons why exceedingly foamed cement caused a notable shift in E_{corr} value to a more negative site. This means that there was a lower coverage by cement's remnants over the steel, and less activity in inhibiting the cathodic corrosion reaction, thereby diminishing the effectiveness of cement in preventing the corrosion of the steel. In contrast, the non-foamed cement better adhered to the steel, suggesting that a strong interfacial bonding of cement developed at the interfaces might act as a barrier layer to minimize the transport of brine to the underlying steel.

Another important factor affecting the mitigation of corrosion by cement is its conductivity of corrosive electrolytes; namely, the extent of the uptake of electrolytes by cement plays a pivotal role in inhibiting or accelerating the corrosion of underlying steel. To obtain this information, thick layers of non-foamed and foamed cements (~1.0 mm to ~1.2 mm) were deposited on the 65 mm × 64 mm steel panels using the same coating process as that employed in the potentiodynamic polarization test, but repeating it three times. The cement-coated steel panels were mounted in a holder, and then inserted into an flat electrochemical cell. The coated panels with a surface area of 13 cm^2 were exposed to an aerated 1.0 M sodium chloride electrolyte at 25 °C for 10 min before the EIS test. As is well documented by several investigators [13–15], the EIS was used extensively for studying the hydration process of cement pastes and the microstructure of porous cementitious systems by measuring the conductivity of pore fluid containing ionic species in the porous cementitious structure. The EIS also was applied to monitoring the corrosion process of reinforcing steel by penetrating chlorides through the porous concrete [16]. In this study, the semicircle diameter at a low-frequency range of 1 mHz to10 Hz in the Nyquist diagram was targeted to determine the pore resistance, R_p, of concrete; namely, the decrease in R_p value corresponded to the increasing rate of corrosion of the reinforcing steel. Based upon this information, we employed frequency range of 10 KHz to 10^{-2} Hz and tried to obtain the R_p value from the Bode-plot diagram. Fig. 10 compares the Bode-plot features [the absolute value of impedance $|Z|(\Omega cm^2)$ vs. frequency (Hz)] of the panels coated with non-foamed cement, and 1, 3, and 20 wt.% reagent-foamed cements. Particular attention in the overall EIS curve was given to the R_p, which can be determined from the peak in the Bode-plot occurring at sufficiently low frequency between 10^{-1} and 10^{-2} Hz [17]. For the non-foamed cement-coated panel, the R_p value was 3.1×10^2 Ωcm^2. When the 1 wt.% reagent-foamed cement was deposited on the panel's surface, the R_p value declined somewhat to 2.4×10^2 Ωcm^2. A further decline to 1.3×10^2 Ωcm^2 was noted from the 3 wt.% reagent-foamed cement, while the 20 wt.% foamed cement showed a very low R_p value of more than one order of magnitude lower than that of the non-foamed cement. Since the R_p value reflects the magnitude of ionic conductivity generated by the NaCl electrolyte passing through the coating layers, such a falling value represented that the uptake of electrolytes by the cement coating was increasingly enhanced as more foaming reagent was added to the cement. Although the Bode-plot curves of 5 and 10 wt.% reagent-foamed cements did not represent in Fig. 10, the Fig. 11 shows the values of R_p value for 0, 1, 3, 5, 10, and 20% foaming reagents. The data clearly verified that an increase in the extent of foaming allowed electrolytes to permeate more easily through the cement layers because of a lowering of R_p with increasing reagent content. In the other words, the enhanced extent of foaming progressively diminished the cement's maximum efficacy as corrosion-preventing barrier layer.

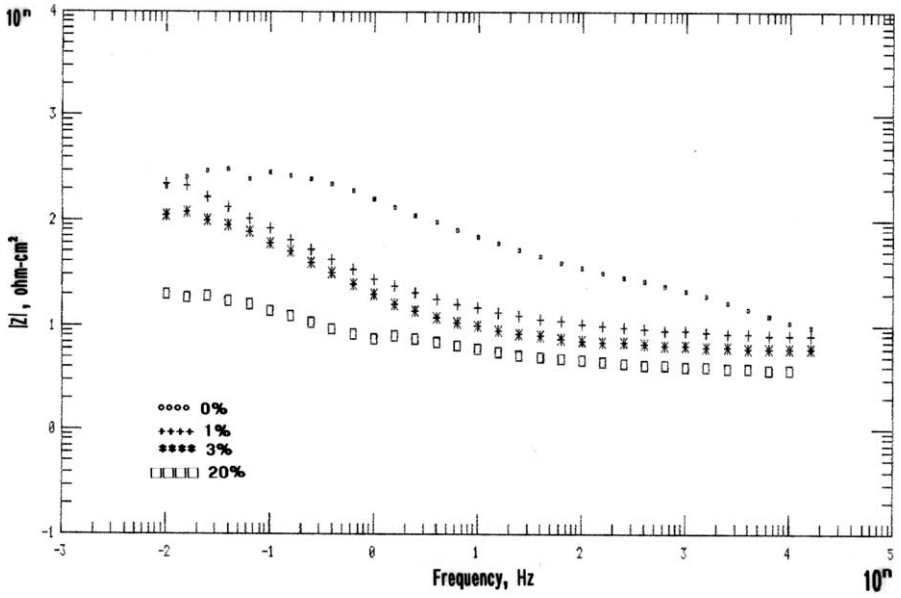

Fig. 10. AC electrochemical impedance curves for carbon steel coated with non-foamed cement, and 1, 3, and 20 wt.% reagent-foamed cements.

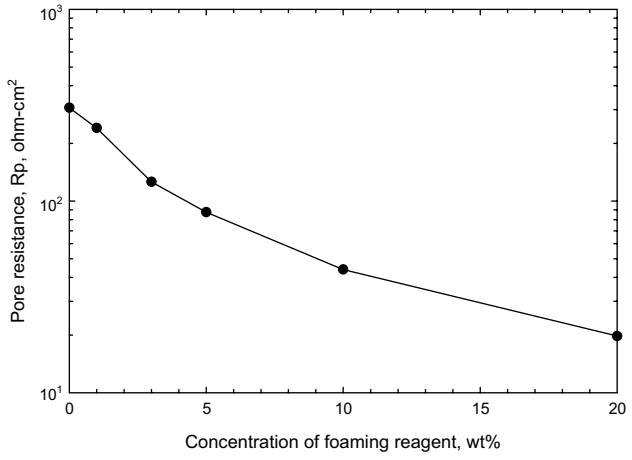

Fig. 11. Changes in pore resistance, R_p, of foam cement-coated steels as a function of the content of foaming reagent.

4. Conclusions

The chemical foaming reagent, which incorporates fine air bubble cells into the cement slurry, significantly contributed to reducing the density of the calcium aluminate phosphate (CaP) geothermal well cement slurry. Using such low-density cement slurry would resolve the problem of lost circulation. When the foamed CaP cement slurries were autoclaved at 200 °C, most of the air bubbles dispersed throughout the slurry led to the development of a porous structure exhibiting a uniform distribution of discrete pores (ranging from ~290 μm to ~40 μm) in the set foam cement. Although the foaming reagent acted to inhibit the extent of reactions between monocalcium aluminate ($CaO.Al_2O_3$) as the major phase in the calcium aluminate cement (CAC) solid reactant, and sodium polyphosphate (NaP) liquid reactant, the three crystalline phases, hydroxyapatite [$Ca_5(PO_4)_3(OH)$, HOAp], boehmite, (γ-AlOOH), and hydrogarnet, ($3CaO.Al_2O_3.6H_2O$, C_3AH_6), as hydrothermal reaction products at 200 °C, were responsible for strengthening the foamed CaP cement. These reaction products offered the improved compressive strength and reduced porosity of the foamed cement, compared with those of N_2 gas-foamed Class G cement made from slurry of similar density. However, adding an excessive amount of foaming reagent dispersed undesirable coalescent bubble cells in the slurry, reflecting the conformation of continuous pore structure in set foam cement. This finding also suggested that the size of bubble cells created by the N_2 gas-foaming technology under high pressure probably was smaller than that of air bubble cells made under no pressure. Thus, one major issue was the increase in water permeability of the cement along with the reduction in the slurry's density, raising concern that the maximum efficacy of cement in mitigating the corrosion of carbon steel well casing pipes was diminished. For non-foamed CaP cement with a porosity of less than 11% and minimum water permeability, the three factors contributed to alleviating the brine-caused corrosion of carbon steel; (1) the excellent adherence of the cement layer to steel, providing a high coverage over the entire steel's surfaces at the interfacial contact zone between the cement and steel, (2) its retardation of the cathodic corrosion reactions, and, (3) its minimum conductivity of corrosive ionic electrolytes. Unfortunately, such efficacy of the

cement in mitigating corrosion was diminished by increasing the extent of its foaming. The most effective amount of this foaming reagent in minimizing this loss of effectiveness and in reducing the slurry's density was 3% by weight of total water in the slurry. Adding this amount gave a slurry density of 1.43 g/cc, which is 25% lower that that of non-foamed slurry, good compressive strength of 24.1 MPa, low water permeability of 1.6×10^{-3} Darcy, and moderate adherence to steel.

References

[1] Sugama T, Wetzel E. Microsphere-filled lightweight calcium phosphate cements. J Mater Sci 1994;29:5165–76.
[2] Moore R, Oil M, Bour D, Reed S, Hemandez R. High-temperature wells with lost-circulation demands and reverse circulation placement techniques using foamed cement systems: Two case histories. Soc Petro Eng SEP 84563, 2003, pp. 69–77.
[3] Montman R, Sutto DL, Harms WM, Mody BG. Low-density foamed portland cements fill variety of needs. Oil Gas J 1982:209–16. July.
[4] Hoff GC. Porosity-strength considerations for cellular concrete. Cem Concr Res 1972;2:91–100.
[5] Brezny R, Green DJ. Factors controlling the fracture resistance of brittle cellular materials. J Am Ceram Soc 1991;74:1061–5.
[6] Tonyan TD, Gibson LJ. Structure and mechanics of cement foams. J Mater Sci 1992;27:6371–8.
[7] Richard TG. Low temperature behavior of cellular concrete. ACI Journal, April 1977:173–7.
[8] Tikalsky PJ, Pospisil J, MacDonald W. A method for assessment of the freeze-thaw resistance of performed foam cellular concrete. Cem Concr Res 2004;34:889–93.
[9] Harms WM, Febus JS. Cementing of fragile-formation wells with foamed cement slurries. Soc Petro Eng SPE 12755, 1984, pp. 277–88.
[10] Montman R, Sutto DL, Harms WM, Mody BG. Low density foam cements solve may oil field problems. World Oil 1982: 171–84. June.
[11] Bozich MP, Montman RC, Harms WM. Application of foamed portland cement to deep well conditions in west Texas. Soc Petro Eng SPE 12612, 1984, pp. 47–53.
[12] Sterm M, Geary AL. Electrochemical polarization I.A theoretical analysis of the shape of polarization curves. J Electrochem Soc 1957;104:56–62.
[13] McCarther WJ, Garvin S. Dependence of electrical impedance of cement-based materials on their moisture condition. J Phys D: Appl Phys 1989;22:1773–6.
[14] Christensen B, Mason TO, Jennings HM. Influence of silica fume on the early hydration of portland cements using impedance spectroscopy. J Am Ceram Soc 1992;75:939–45.
[15] Xu Z, Gu P, Xie P, Beaudoin JJ. Application of AC impedance techniques in studies of porous cmenetitious materials (III): ACIS behavior of very low porosity cementitious systems. Cem Concr Res 1993;23:1007–15.
[16] Poupard O, Ait-Mokhtar A, Dumargue P. Corrosion by chlorides in reinforced concrete: Determination of chloride concentration threshold by impedance spectroscopy. Cem Concr Res 2004;34: 991–1000.
[17] Mansfeld F, Kendig MW, Tsai S. Evaluation of corrosion behavior of coated metals with AC impedance measurements. Corrosion 1982;38:478–85.